# EXPERIMENTAL AND NUMERICAL INVESTIGATION OF THE DROPLET BEHAVIOR PASSING A COMPRESSOR CASCADE

B. Ober*, C. Storm*, H. Gomaa°, S. Seifert°, B. Weigand°, F. Joos*

*Laboratory of Turbo Machinery / Power Engineering
Helmut Schmidt University / University of the Federal Armed Forces; 22043 Hamburg, Germany
°Institute of Aerospace Thermodynamics
University of Stuttgart; 70569 Stuttgart, Germany

**ABSTRACT**

High fogging systems are often used in gas turbine power stations for power augmentation. Water droplets injected into the compressor inlet will partly follow the air flow, will partly be splashed at the compressor blades and partly touch the surface of the blades. The water film of the surface will be atomized at the trailing edge of the blade.

The work presented concerns with the numerical calculation of the spray behavior passing a transonic compressor cascade investigating droplet atomization. The physical models used are discussed in detail. The comparison with measurements of the droplet velocity as well as of the droplet size distribution of the transonic two phase flow inside a planar compressor cascade explains the accuracy of the physical models used in the numerical investigation.

## INTRODUCTION

The ongoing change towards the use of renewable sources of energy imposes new challenges to the grid with regard to grid stability. Presently available storage capacity is not sufficient to stabilise the fluctuating power output of electric energy sources such as wind or solar. In order to cope with these fluctuations an energy supply system is needed that is able to adapt quickly to the demand. Gas turbines have, due to their short start up times, proven a reliable support in ensuring a stable grid. But yet a more efficient and more capable gas turbine system remains desirable. One way to augment the power output and increase the efficiency of a gas turbine is the injection of water droplets into the inlet structure (1).

The mechanisms that determine the behaviour of the water spray in the compressor of a gas turbine are not yet fully understood. Moreover remains the testing in this field of research demanding because of the efforts that have to be taken with regard to energy consumption and equipment (2). Therefore the implementation and validation of numerical test methods is a key milestone on the road to employ the entire potential of this technology.

In order to take the development one step further the authors have conducted numerical and experimental investigations on the droplet behaviour passing a compressor cascade.

## APPROACH

The Laboratory of Turbo Machinery at the Helmut Schmidt University in Hamburg, Germany possesses a high speed wind tunnel. The results obtained during the experimental investigations conducted at this test facility serve as the data basis for the numerical investigations for which two different approaches were chosen. One study dealt with two existing particle breakup models implemented in AVL Fire which aimed at the assessment of the general behaviour and flexibility of the respective model. Within the second study a standalone model that communicates directly with ANSYS CFX was tested to clarify its suitability to predict the prevalent phenomena in a cascade flow. The calculations conducted in Stuttgart used Fire by AVL. In Hamburg a self developed code for the dispersed phase (DPF) which communicates with ANSYS CFX was used. Both packages utilize the Navier-Stokes-Equations which will not be discussed in detail in this work. Further information can be found in various publications (3).

## EXPERIMENTAL INVESTIGATION

### Test Rig

The wind tunnel which is capable of delivering supersonic flow regimes consists of the major components:

- centrifugal compressor
- settling chamber
- intake duct with film layer injection
- cascade
- water separator

The basic setup is depicted in Figure 1.

The compressed air supplied by the centrifugal compressors (not depicted) is fed into the settling chamber where the flow is equalised. The compressors are capable of delivering a supercritical pressure ratio. The maximum Mach number in the test section is Ma=1.2. A high pressure pump atomizes desalinated water into the settling chamber.

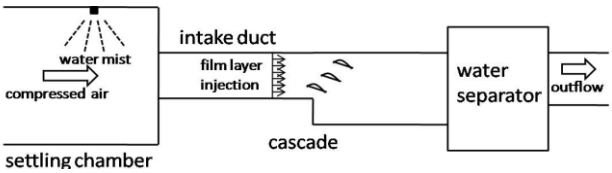


**Figure 1:BASIC SETUP OF TEST RIG (4)**

Constructional boundary conditions demand an intake duct of *l*= 2m. The imposed boundary layer has to be accounted for during two dimensional testing. This is achieved by a film layer injection which accelerates the flow close to the side walls.

The test section is depicted schematically in Figure 2. It contains a compressor blade cascade of nine controlled diffusion airfoils. The blade contour is derived from a cross section of an actual axial compressor profile which has been extruded. Glass windows allow optical accessibility.

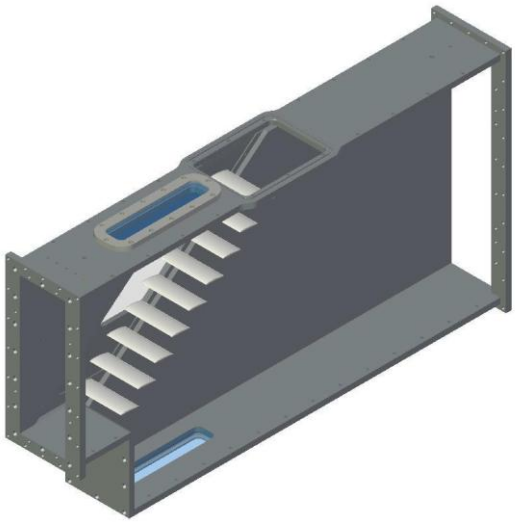

**Figure 2: TEST SECTION (4)**

## Measurement technique

Test results comprise of velocity and diameter information of the droplets passing the cascade. A two dimensional Laser Doppler Anemometry and Phase Doppler Anemometry setup (2D LDA/PDA) delivers the necessary information. The light source is an argon ion laser with a power output of 4W.

The field of interest is captured in a point to point measurement with 1200 nodes. The dry flow is examined with 2000 samples and 5000 for the droplet laden flow respectively. The velocity information of a dry flow is recorded with the use of Di-Ethyl-Hexyl-Sebacat (DEHS) droplets which can be easily atomized to sizes which are known to follow the air flow with negligible deviation $(d < 0.3\ \mu\text{m})$ (1).

## Droplet classification

The diameter distribution can be evaluated by the use of the Sauter-Mean-Diameter (SMD) $D_{32}$ . It is given by:

$$D_{32} = \frac{\sum_{i=1}^{N} n_i d_d^3}{\sum_{i=1}^{N} n_i d_d^2} \qquad (1)$$

Herein $N$ is the number of droplet size classes, $n_i$ is the number of particles in the respective size class and $d_d$ is the corresponding diameter. The SMD is a useful measure to analyse droplet behaviour with regard to evaporation as it is the ratio of the dispersed phase's volume and surface.

A characteristic flow induced by a Controlled Diffusion Airfoil (CDA) incorporates a regime of high velocity on the suction side of the profile. Therefore the description of droplet behaviour has to consider three phenomena in the compressor application.

## Experimental data

The measurements were carried out by (4) using the parameters:

**Table 1: CASCADE FLOW CONDITIONS**

| Parameter | Value |
|---|---|
| Mach number | 0.85 |
| Reynolds number | 673000 |
| Temperature | 293 K |
| Total pressure | 1260 mbar |
| AVDR | ≈ 1.08 |
| Flow angle $\beta_1$ | 35.6 deg |
| incidence | 0 deg |

Results of the dry reference air flow show a typical velocity distribution of a compressor profile of this type as depicted in Figure 3. The incident flow is accelerated on the suction side of the profile and forms a transonic flow regime. Further downstream the flow is decelerated to subsonic velocities. Most characteristic for this type of blade is the rapid acceleration which imposes high relative velocities to any inert particle passing the area.

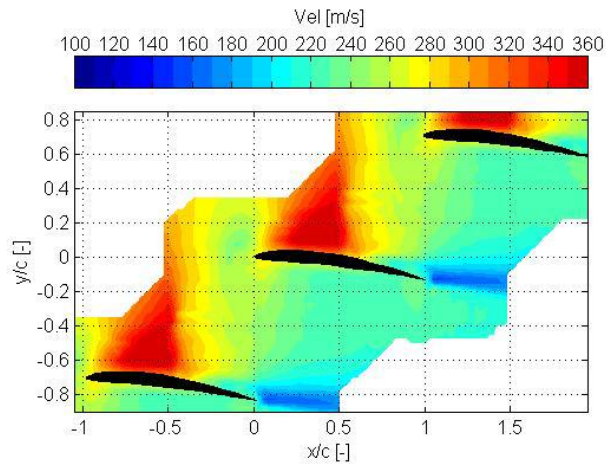


**Figure 3: EXPERIMENT: DRY AIR (4)**

The effects can be seen in Figure 4. Depicted is the SMD of a droplet laden flow. The results show a quasi uniform diameter distribution at the cascade entrance of 50-55 µm. In the area which is characterized by transonic velocities in Figure 3 a decrease in SMD is observed.

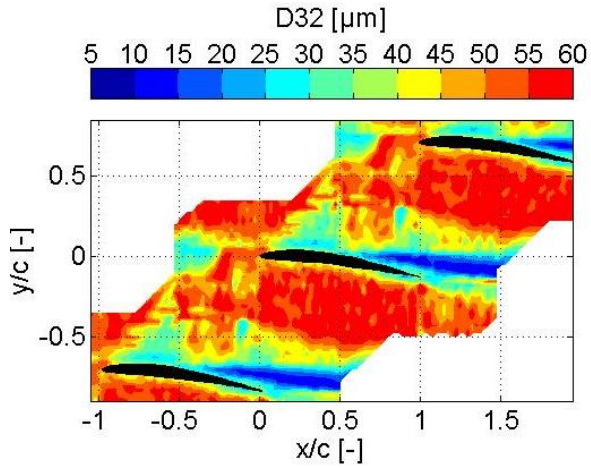


**Figure 4: EXPERIMENT: SMD (4)**

Calculations of the Weber number based on the relative velocity and a mean droplet diameter $d = 20...40\ \mu m$ (Figure 5) however show a maximum value of $We_{max} = 3$ which is well below the critical value of $We_{crit} = 12$ for droplet breakup (5). Based on this information it can be assumed that breakup does not occur for $d_d \leq 40\ \mu m$. The discrepancy between measurement and phenomenological investigation can be justified with the inability of PDA to account for deformed droplets and the sensitivity of SMD calculation to large diameters as (4) reported. The influence on much larger droplets are not yet quantified. Future investigations will have to clarify the critical droplet diameter for s to occur. Downstream of the transonic flow regime a reduced SMD of $D_{32} = 5...15\ \mu m$ is recorded. This is partly due to small droplets as a result of the splashing phenomenon on the leading edge of the blade and partly due to the water film disintegration on the suction side.

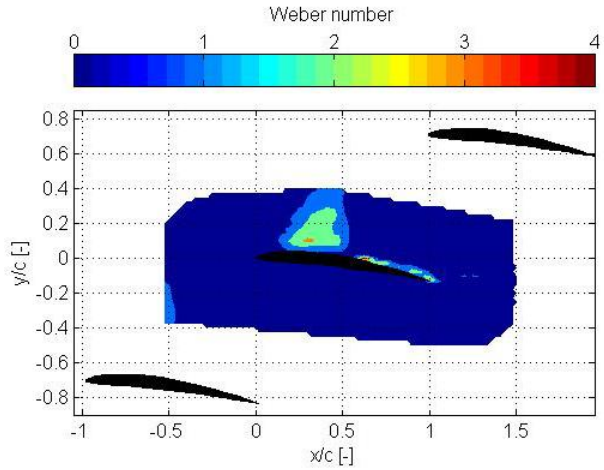


**Figure 5: EXPERIMENT: WEBER NUMBER 20-40µm (4)**

## MODEL TEST: NUMERICAL INVESTIGATION OF A SINGLE AIRFOIL

### AVL Fire

Desired applications of a numerical model for droplet breakup in axial compressors include a wide range of possible flow parameters. Especially droplet disintegration will be studied, because this might be important in industrial applications where Ma and Re numbers are higher and the injected droplets are larger than in current tests. The computations utilizing AVL Fire focus on model studies. Hence, a simplified geometry, namely a single compressor profile shaped airfoil, depicted in Figure 6, has been selected. This is suitable for investigating various models for disintegration and atomization.

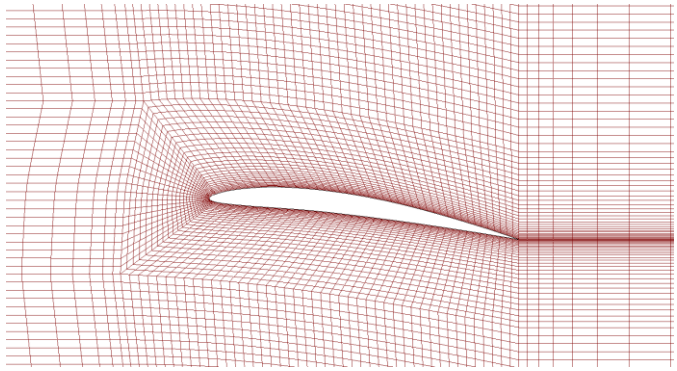

**Figure 6: SIMULATION: AREA OF INTEREST**

Restrictions in computing capacity for calculations with AVL Fire demanded to restrict the computed area to a flow passage around the blade instead of the entire cascade. The boundary conditions are derived from experimental data.

A full run of a two phase flow simulation consists of three steps:

- calculation of dry flow
- calculation of droplet laden flow without breakup
- calculation of droplet laden flow with breakup

Calculation of the dry flow is necessary to find the proper boundary conditions for the two phase flow. From a calculation of a droplet laden flow with disabled breakup model the distribution of relative velocity between phases is derived. This information is then fed into the simulation including breakup modelling as it is a necessary set of information for the calculation.

For the simulation of the dry flow total pressure at the inlet is adjusted until the velocity distribution matches the experimental data. The resulting Ma number distribution is depicted in Figure 7.

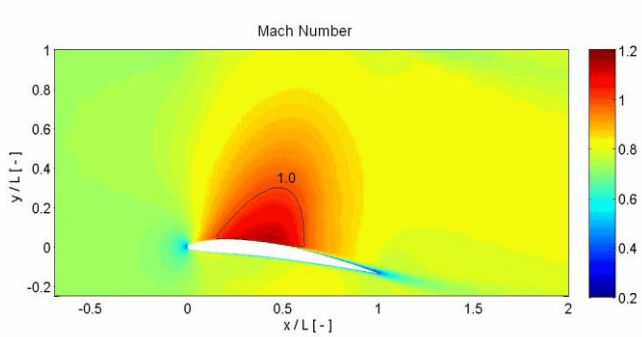


**Figure 7: SIMULATION: MACH NUMBER DRY AIR**

The incident velocity is uniformly distributed at $237$ m/s. Flow is accelerated on the suction side of the profile up to transonic velocities. Further downstream a deceleration to $v > 250$ m/s can be observed. In contrast to experimental data the velocity at the trailing edge is greater than at the leading edge of the blade, which is abnormal for a compressor

application. This difference is the result of an absent staggering angle which is due to the computational boundary conditions as mentioned above. The similarity with regard to the transonic flow regime remains.

AVL Fire delivers the functionality to conduct a simulation of the described kind. An Euler-Lagrangian approach is used. Breakup models like WAVE and TAB are already implemented. The investigation of the breakup models aimed at the clarification whether an adaption to the application at hand is possible.

**Droplet Breakup: WAVE Standard Model**

The Wave model (6) is based on the stability analysis of a cylindrical slab of water as depicted in Figure 8. It was developed for the modeling of primary jet disintegration and also considers secondary breakup. Only the latter is relevant within this study.

An infinitesimal axially symmetric disturbance is exerted upon the surface. The initial displacement of the magnitude $\eta_0$ will grow with a rate of $\omega$. The corresponding wavelength is $\lambda$.

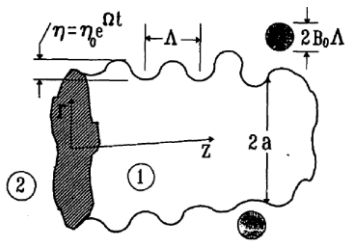


**Figure 8: CONCEPT OF WAVE (6)**

Let the maximum growth rate $\omega_{max} = \Omega$ occur with the corresponding wavelength $\Lambda$. Wavelength $\Lambda$ and growth rate $\Omega$ then characterize the fastest growing wave on the surface. Calculations are conducted with local fluid properties.

$$\frac{\Lambda}{r} = 9.02 \frac{(1+0.45\ Oh_d^{0.5})(1+0.4\ T^{0.7})}{(1+0.87\ We_g^{1.67})^{0.6}} \quad (2)$$

$$\Omega \left( \frac{\rho_g r^3}{\sigma} \right)^{0.5} = \frac{0.34+0.38\ We_g^{1.5}}{(1+\ Oh_d)(1+1.4\ T^{0.6})} \quad (3)$$

where

$$We_g = \frac{u_{rel}^2 r \rho_g}{\sigma}, \quad (4)$$

$$Oh_d = \frac{\eta_d}{\sqrt{\rho_d r \sigma}} \quad (5)$$

and

$$T = Oh_d We_g^{0.5}. \quad (6)$$

Disintegration is then accounted for by the formation of new stable droplets which are sheared off the surface. The radius of the new droplet is $r_{stable}$ and the rate of change in radius of the original droplet is denoted by

$$\frac{dr}{dt} = \frac{-(r - r_{stable})}{\tau_a} \quad (7)$$

wherein

$$\tau_a = \frac{3.726 C_2 r}{\Lambda \Omega} \quad (8)$$

is the duration of the disintegration process. For the investigations conducted here only the secondary breakup is relevant. The size of the secondary droplet is assumed to be proportional to $\Lambda$. The radius is then:

$$r_{stable} = C_1 \Lambda \quad (9)$$

The breakup only occurs if $C_1 \Lambda \leq r$. Duration of breakup process is computed using:

$$t_2 = C_2 \frac{r}{u_{rel}} \left( \frac{\rho_d}{\rho_g} \right)^{0.5} \quad (10)$$

Constant $C_1$ influences the model's behaviour with regard to the predicted size of the secondary droplet (eqn. (9)). By adjusting the value of constant $C_2$ the duration of disintegration is altered (eqn. (10)). A parameter study has been conducted to indentify the most suitable combination for the problem at hand. The results of the two phase flow simulation using the pressure boundary conditions found in the simulation of the dry flow are depicted in Figure 9.

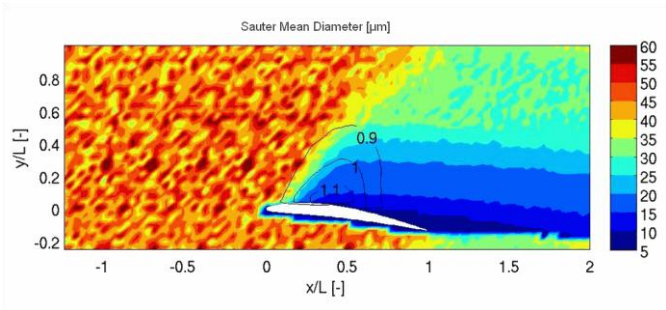


**Figure 9: SIMULATION: WAVE RESULTS**

The incident flow is characterized by a non uniform SMD-distribution of $D_{32,inc} = 35...60\ \mu m$ and a regular pattern of high and low values. The boundary conditions are chosen according to the experimental data ($D_{32,inc} = 45\ \mu m$) and the injection of droplets is done randomly. Other than expected, the SMD is not homogeneous, indicating a not completely random inflow of droplets.

Particle breakup is predicted in the area of transonic flow regime. The relative velocity in this area exceeds stability threshold of $v_{rel} \leq 40$ m/s as derived from the parameter studies. In comparison to experimental data it can be stated that SMD in subsequent flow is generally underestimated. The resulting SMD increases with increasing distance from the blade surface in vertical direction corresponding to the decreasing relative velocity in the same direction as depicted in Figure 10. The number of constants that influence the model's behavior proved to be insufficient to adjust droplet breakup with regard to point in time, duration and secondary droplet size independently.

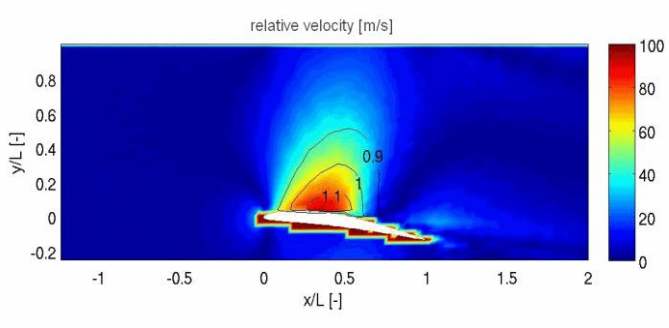


**Figure 10: SIMULATION: RELATIVE VELOCITY**

### Droplet Breakup: Taylor Analogy Breakup Model

An oscillating droplet's movement is analyzed in analogy to the standard spring-damper model as formulated by (7) (Figure 11). The underlying law of movement is formulated:

$$m\ddot{x} = F - kx - d\dot{x}. \tag{11}$$

In this application $x$ is the excitation of the droplet's equator, as depicted in Figure 12.

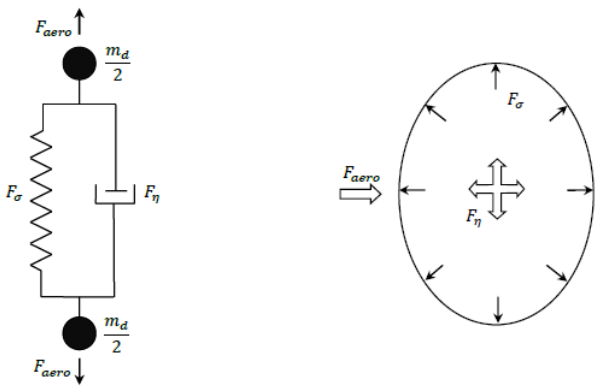


**Figure 11: TAB: SPRING MASS ANALOGY (7)**

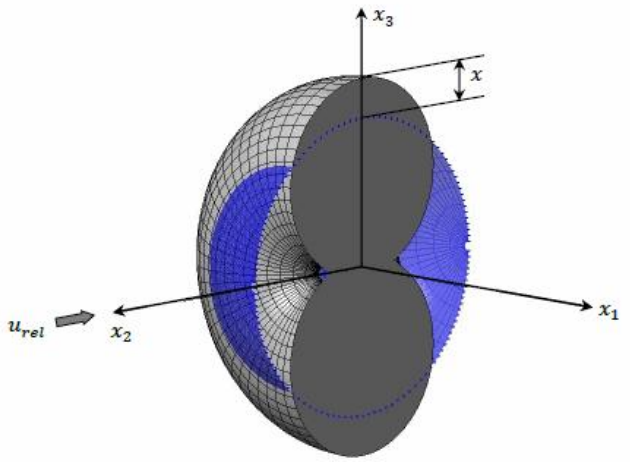


**Figure 12: TAB: DROPLET DEFROMATION (7)**

It is assumed that breakup occurs if $x > C_b r$. Herein $C_b$ is a dimensionless constant. The dimensionless displacement of the droplet's equator is:

$$y = \frac{x}{C_b r}. \tag{12}$$

It is further assumed that the external force is equal to the force exerted by the continuous phase, that the force exerted by the spring is equal to the surface tension and that the damping force is equal to the viscosity of the fluid. Equations and the assumptions above yield:

$$\ddot{y} = \frac{C_F \rho_g u^2}{C_b \rho_d r^2} - \frac{C_k \sigma}{\rho_d r^3} y - \frac{C_d \eta_d}{\rho_d r^2} \dot{y}. \tag{13}$$

Constants $C_i$ are determined via mathematical analysis and experimental data. The original droplet oscillates normal to the direction of movement. If $y > 1$ the droplet disintegrates and new droplets are formed. The size of the secondary droplet is determined via the law of energy conservation. The sum of the droplet's energy comprises surface-, oscillation- and deformation energy.

$$E_{original} = 4\pi r^2 \sigma + \frac{\pi}{5} \rho_d r^5 (\dot{y} + \omega^2 y^2) \tag{14}$$

Herein is $K$ the ratio of deformation and oscillation energy to energy in fundamental mode. Secondary droplets are assumed to be spherical and stable. Therefore the total energy of secondary droplets consists of surface and kinetic energies:

$$E_{product} = 4\pi r^2 \sigma \frac{r}{r_{32}} + \frac{\pi}{6} r^5 \rho_d \dot{y}^2 \tag{15}$$

Equalization yields:

$$\frac{r}{r_{32}} = 1 + \frac{8K}{20} + \frac{\rho_d r^3}{\sigma} \dot{y}^2 \left( \frac{6K - 5}{120} \right) \tag{16}$$

Constant $K$ can be adjusted to deliver the desired secondary droplet size.

The model's sensitivity to different values for each factor $C_i$ has been investigated in a parameter study. The results of a simulation utilizing the most suitable combination of constants is depicted in Figure 13

The incident flow shows the same properties as seen in the

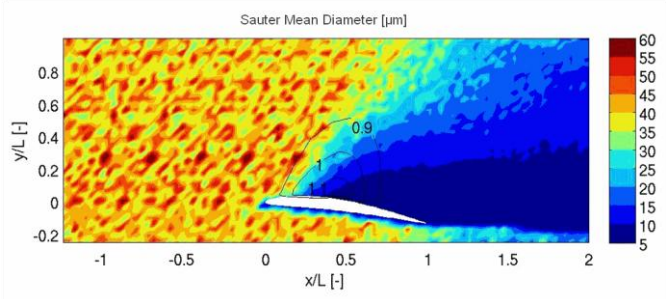


**Figure 13: SIMULATION: TAB RESULTS**

previous investigation using the WAVE model. Again a non uniform SMD distribution is visible as well as a regular pattern in the incident flow. Values for SMD are again underestimated in comparison to experimental data in the region downstream of the transonic flow regime. Even though the TAB model has a more versatile set of adjustment parameters a strong cross influence between the parameters remains. The influence of the parameters on the different aspects of droplet breakup (point in time, duration and secondary droplet size) proved to be too widespread to achieve a suitable combination. To be able to arbitrarily adapt the breakup properties enhanced modeling is necessary. Therefore a set of parameters that have an isolated influence on each aspect of droplet breakup is desirable.

## NUMERICAL INVESTIGATION OF A COMPRESSOR CASCADE

### Disperse Phase Flow Code (DPF)

The Disperse Phase Flow (DPF) Code first introduced by (8) is a FORTRAN written source code designed for communication with the ANSYS CFX 13.0 flow solver for numerical simulation of water droplet-laden compressor flows. Utilising an Euler-Lagrange approach the two phases are considered separately. Source terms, as resultant forces of momentum, are determined from droplet motion within the DPF code and considered in the ANSYS flow solver calculations for the continuous phase to obtain a two-way coupling. The successive computation facilitates stability and efficiency, while flexibility is maintained by the independent and expandable routine structure of the FORTRAN Code.

The turbulent continuous phase is calculated by ANSYS CFX 13.0 utilizing a finite volume discretization scheme to solve Reynolds averaged Navier Stokes equations associated with the k-ε turbulence model for closure. Via the ANSYS User Fortran interface the DPF Code initiates the read-out of fluid flow data followed by the successive calculation of droplets' trajectories within the computational mesh. The forces of the carrier flow acting on a particle i.e. drag force $F_{CW}$, force of gravity $F_G$, pressure gradient force $F_P$, virtual mass force $F_{VM}$, basset force $F_B$ and forces due to domain rotation $F_R$, deliver the equation of motion:

$$m_d \frac{du_{d,i}}{dt} = F_{CW,i} + F_{G,i} + F_{P,i} + F_{VM,i} + F_{B,i} + \dots \quad (17)$$

(i: index for Cartesian coordinate)

For consideration of droplet specific phenomena, disperse phase models for turbulent dispersion, secondary breakup and splashing are implemented within discrete routines as (8) presented.

To model the turbulent dispersion due to turbulent fluctuations of the carrier flow a stochastic method, i.e. the eddy interaction model concept mainly described by (9) is applied by that particle interaction with a succession of fluid phase turbulent eddies is simulated. Turbulent kinetic energy k and the energy dissipation rate ε of the continuous phase are taken for estimation of the current eddy's life time $T_e$ and length scale $L_e$. Not until the droplet leaves the eddy or the eddy collapses a new eddy is considered. For the duration of particle eddy interaction the fluctuating part of the particle velocity is determined on the basis of a Gaussian distribution with zero mean. Under assumption of isotropic turbulence the variance is directly derived from the definition of turbulent kinetic energy.

A rather droplet specific behaviour is the deformation due to aerodynamic load acting. Depending on flow velocities, fluid properties and particle diameter, the extent of deformation affects its resistance coefficient and hence particle motion but further leads to secondary breakup as a result of exceedingly high deformation. The DPF code accounts for this behaviour by means of the Taylor Analogy Breakup (TAB) model introduced by (7) as described above. To define the critical value of deformation at which secondary breakup occurs an empirical model by (10) is introduced. In dependence of the Weber number and taking nonlinearities of acting forces and deformations at larger deformations into account, following equation with upper boundary of deformation $y_{c,max}$ =2.1 and lower boundary of deformation $y_{c,min}$=1.771 is implemented:

$$\begin{aligned} We \le 13 \quad & y_c = y_{c,min} \\ We > 13 \quad & y_c = y_{c,min} + (y_{c,max} - y_{c,min}) \\ & \cdot \left[ 1 - \exp\left( - \frac{We - We_c}{2} \right)^{1.2} \right] \end{aligned} \quad (18)$$

In consequence of droplet breakup secondary droplets are generated by dynamic allocation of memory within the DPF code. The same principle is applied on splashing occurrence.

The simulation model for droplets impinging on dry or wetted surfaces need to imply splashing and deposition mechanisms. The implemented model by (11) applies a criterion for splashing with account to wet surfaces, by use of the film thickness h, and based on the *K* value, which was first introduced by (12).

$$K^2 = \frac{\rho u_{pri}^2 d_{pri}}{\sigma} \frac{1}{\min\left( \frac{h}{d_{pri}}, 1 \right) + \frac{1}{Re_n^{0.5}}} > K_c^2 \quad (19)$$

For dry surfaces as regarded in the validation calculations the criterion for splashing agrees with the formulation by (12) and the critical *K* value of $K_{crit}$ = 57.7. Further (10) introduced empirically derived correlations for the mass fraction of secondary to primary droplets as well as for secondary droplet diameter and velocities. For estimation of the secondary droplets' diameter, fluctuation velocities and circumferential angle a Nukiyama-Tanasawa distribution function is utilised in addition.

For validation purposes a droplet laden compressor flow according to the experimental investigations has been simulated. The computational quasi-two-dimensional domain contains the three centre blades of the transonic compressor cascade which are embedded within an ANSYS ICEM mesh grid of 114,000 hexahedral cells utilising C-grid structures. Experimental flow conditions are applied by defining the total pressure and total temperature condition at the inlet and a static pressure at the outlet. Regarding the restricted dimensions of the computational domain symmetry conditions are set at the side planes and periodic conditions at the lower and upper boundary as shown in figure 14.

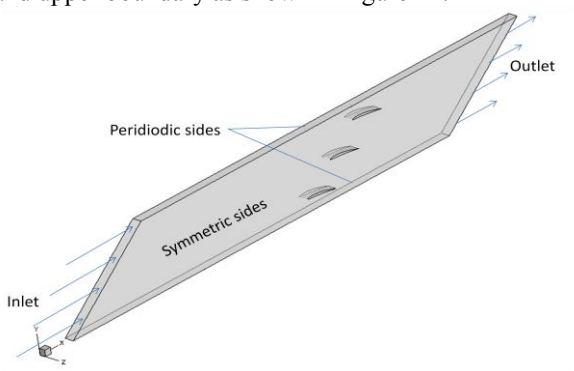


**Figure 14: BLADE PASSAGE DOMAIN (13)**

First simulations of the dry air compressor flow for evaluation of the continuous phase are opposed to corresponding experimental measurements. Both cases revealed good agreement concerning the transonic regime, with a supersonic flow region on the suction side terminated

by a shock inducing flow separation, except a thinner wake region and less boundary layer thickening remained noticeable. More accurate results may be obtained by higher grid resolution or another turbulence model for better boundary layer treatment, but both options are not applicable in connection with the FORTRAN source code, so that minor variations are considered negligible.

For the droplet-laden compressor flow additional boundary conditions concerning the disperse phase are set within the DPF code environment. The experimental measured diameter spectrum is applied for the inlet flow of the droplets with a given water load of 2% of the air mass flow and an approximated number of 50,000 trajectories. The numerical results of both phases are joined using the visualisation software TECPLOT 360 2010.

Corresponding to the experimental results the distribution of the SMD is plotted as depicted in Figure 15.

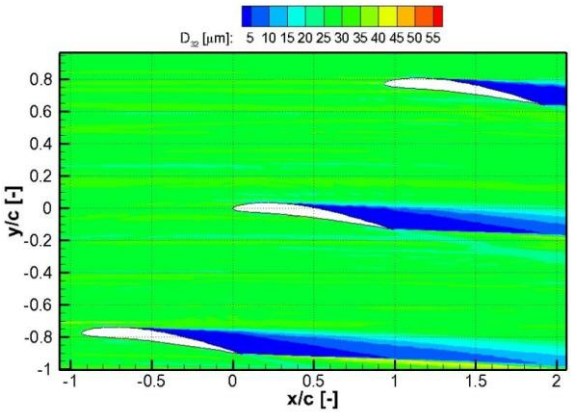


**Figure 15: SIMULATION: SMD UTILISING DPF**

The numerical computations reveal a homogeneous distribution of the $D_{32}$ diameter on the pressure side as well as on the suction side, but an accumulation of particles with lowest mean diameters in the separation area and wake. Since no evaporation model is implemented droplet size remains constant along the trajectories, except if splashing or secondary breakup occurs. However for the given droplet diameter spectrum secondary breakup is not observed during numerical computations. Hence the droplets of lower diameter accumulated in the separation area and wake result of splashing only.

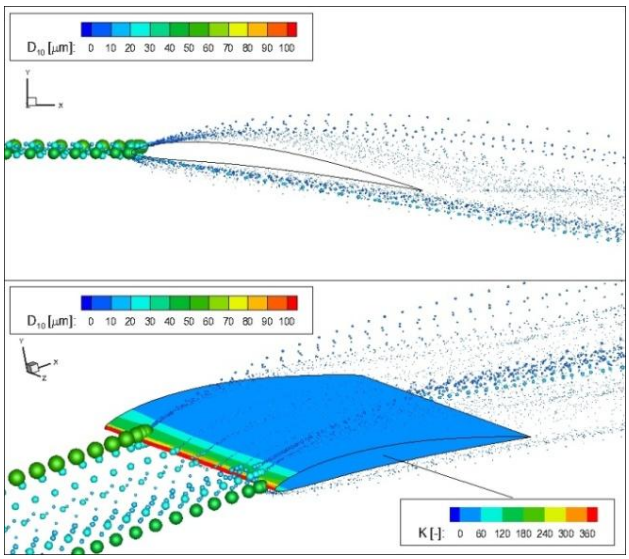


**Figure 16: SIMULATION: SPLASHING DROPLETS (13)**

Figure 16 depicts the process of several droplets splashing on the leading edge of the blade depending on the present $K$ value. Splashing criterion is met above $K_c = 57.7$ resulting in multiple secondary droplet trajectories. Rebounding secondary droplets follow the airflow according to their inertia and lower particle relaxation time with quick adaptation to the near surface flow of the continuous phase towards the trailing edge.

In consequence the secondary droplets of reduced diameter accumulate in the wake of the blade while the larger primary droplets dominate in the flow to the opposed blade.

In qualitative comparison to the experimental measurements shown in Figure 4, similar results are obtained numerically with a homogeneous pattern of the diameter distribution along the blade's pressure side and accumulation of the lowest droplet diameter in the separation area and wake. The discrepancy within the transonic flow regime at the suction side, revealing measurements of reduced droplet diameter, were declared to be underestimated as described above.

## CONCLUSIONS

The investigations conducted dealt with the behaviour of liquid droplets passing a transonic compressor cascade experimentally and numerically. Experiments carried out at the test facility at the Helmut-Schmidt-University in Hamburg, Germany served as the data basis for numerical investigations. The goal of the numerical investigations had two aspects. On the one hand the adjustability of the WAVE and TAB model was tested to assess the flexibility with regard to different aspects of droplet breakup. On the other hand a standalone code (DPF) was tested with regard to its ability to predict the droplet's behaviour in a compressor cascade.

Results show that the main properties of droplet breakup in a simulation, that are breakup location, breakup time as well as the resulting droplet diameters, are adjustable. This is done via the adjustment of the model's parameters. However, it is not possible to adjust them independently from each other, leading to a coupling of the properties.

The combination of ANSYS CFX and the in house developed code DPF was used to simulate a cascade flow in analogy to the experiments conducted. Due to the integration of a splashing model DPF was able to produce results that show a close correlation with the experimental results, as splashing appeared to be the prevalent driver of droplet diameter change in the flow.

Further prospects include the improvement of DPF to reduce the deviations seen and to include phenomena which are not yet accounted for as droplet collision and deformation.

The determination of a critical droplet diameter for secondary breakup needs further determination as well.

## ACKNOWLEDGEMENTS

The authors would like to thank the DFG for supporting this project.

## NOMENCLATURE

### Latin Symbols

| | | |
|---|---|---|
| C | constant | [-] |
| d | diameter | [µm] |
| D | diameter | [µm] |
| E | energy | [J] |
| F | force | [N] |
| K | constant | [-] |
| l | length | [m] |
| r | radius | [m] |
| t | time | [s] |
| u | velocity | [m/s] |
| x | displacement | [m] |
| y | dimensionless displacement | [-] |

### Dimensionless Numbers

| | | |
|---|---|---|
| Ma | Mach number | [-] |
| Oh | Ohnesorge number | [-] |
| We | Weber number | [-] |

### Greek Symbols

| | | |
|---|---|---|
| β | flow angle | [°] |
| η | dynamic viscosity | [kg/m s] |
| ρ | density | [kg/cm$^3$] |
| σ | surface tension | [N/m] |
| τ | disintegration time | [s] |
| ω | growth rate | [1/s] |
| Λ | wave length | [m] |
| Ω | growth rate | [1/s] |

### Indices

| | |
|---|---|
| 0 | initial condition |
| 1...n | counter |
| 32 | Sauter Mean Diameter |
| B | Basset force |
| CW | drag force |
| d | dispersed (Phase) |
| e | eddy |
| g | gaseous (Phase) |
| G | gravity |
| inc | incidence |
| max | maximum |
| original | original |
| P | product |
| pri | primary |
| product | product |
| rel | relative |
| R | rotation |
| sec | secondary |
| stable | stable |
| VM | virtual mass |

### Abbreviations

| | |
|---|---|
| CDA | Controlled Diffusion Airfoil |
| DEHS | Di-Ethyl-Hexyl-Sebacat |
| DPF | Dispersed Phase Fortran Code |
| LDA | Laser Doppler Anemometry |
| PDA | Phase Doppler Anemometry |
| SMD | Sauter Mean Diameter |
| TAB | Taylor Analogy Breakup |

## LITERATURE


1. **Kleinschmidt, R. V.** Value of wet compression in gas-turbine cycles. *Mechanical Engineering.* 1947, Vol. 69, p. 115-116.

2. **Ober, B., Eisfeld, T. and Joos, F.** *Aerodynamische Untersuchungen an Axialverdichtergittern an der Helmut-Schmidt-Universität Hamburg.* Hamburg : DGLR Jahrestagung 2010 Hamburg, 2010. 1302.

3. **Ferziger, J.H. and Peric, M.** *Computational Methods for Fluid Dynamics.* Berlin, Heidelberg, New York : Springer, 2002. ISBN 978-3-540-67586-0.

4. **Eisfeld, T. and Joos, F.** *Experimental Investigation of Two-Phase Flow Phenomena in Transonic Compressor Cascades.* Orlando, USA : ASME Turbo Expo 2009, 2009. GT2009-59365.

5. **Schmelz, F.** *Tropfenzerfall in beschleunigten Gasströmungen.* Aachen, Germany : Shaker, 2002. ISBN 978-3-540-71865-9.

6. **Reitz, R. D.** Modeling Atomization Processes in High-Pressure Vaporizing Sprays. *Atomisation and Spray Technology.* 1987, Vol. 3, p. 309-337.

7. **O'Rourke, P. J. and Amsden, A. A.** *The Tab Method for Numerical Calculation of Spray Droplet Breakup.* Toronto : Society of Automotive Engineers, 1987. SAE 872089.

8. **Matysiak, A.** *Euler-Lagrange Verfahren zur Simulation tropfenbeladener Strömung in einem Verdichtergitter* . s.l. : Universität der Bundeswehr Hamburg, 2007. Dissertation.

9. **Gosman, A.D. and Ioannides, E.** *Aspects of Computer Simulation of Liquid-Fueled Combustors.* Vol. 7, No. 6 : J.Energy, 1983. 4852-490.

10. **Schmehl, R.** *Tropfendeformation und Nachzerfall bei der technischen Gemischaufbereitung.* Berlin : Logos, 2004. ISBN 978-3-8325-0707-7.

11. **O'Rourke, P.J. and Amsden, A.A.** *A Spray/Wall Interaction Submodel for the KIVA-3 Wall Film Model.* Detroit, USA : Society of Automotive Engineers, 2000. SAE2000-01-0271.

12. **Mundo, C.** *Zur Sekundärzerstäubung newtonscher Fluide an Oberflächen, Ph.D. Thesis.* Erlangen-Nürnberg : University Erlangen-Nürnberg, 1996.

13. **Storm, D. and Joos, F.** *Euler-Lagrange Method for Numerical Simulation of Water Droplet-Laden Compressor Flows.* Stockholm : ISABE, 2011. 2011-1254 - Accepted Paper.

14. **Eisfeld, T. and Joos, F.** *New boundary layer treatment methods for compressor cascades.* Graz, Austria : s.n., 2009. ETC8 - B250.